CHAPTER 3

The population dynamics of *Ectemnorhinus* weevils from the Prince Edward Island Archipelago

Abstract: *Ectemnorhinus* weevils were collected from diverse localities on the sub–Antarctic Marion (MI) and Prince Edward Island (PEI) of the Prince Edward Archipelago (PEAI). A COI gene phylogeny was inferred for the 187 specimens following nested clade analysis. The results of the nested clade analyses were mapped on the islands on the basis of weevil sampling locality. These results were interpreted with reference to known glacial margins, striae, and moraines of the last glacial maximus on Marion Island, as well as the geology of the islands. As no evidence of glaciation has been found on Prince Edward Island, emphasis was placed on Marion Island. Results indicate that *E. kucheli* originally colonized PEI and subsequently colonized MI before the last recorded glaciation on MI. *Ectemnorhinus similis* evolved in allopatry and almost reached extinction on MI during the last glaciation, being confined to an ice-free region in the south-western corner of the island. Once the ice began melting it appears that *E. similis* was able to re-colonize MI, most likely with the aid of the strong, frequent south-westerly winds. However, subsequent volcanic eruptions most likely pocketed the weevils across the island and the ensuing isolation was sufficient for differentiation of weevils, as a genetic signature of multiple genetically-identifiable populations is apparent. As conditions became favorable, weevils began to migrate in a mostly south-westerly direction consistent with the strong, frequent south-westerly winds. Although individuals from different genetically-identifiable lineages/populations currently have overlapping distributions, no gene flow is evident between them. The analyses also indicate that reverse migration of *E. similis* from MI to PEI occurred. With respect to *E. kucheli*, two genetically distinct populations were identified on PEI. In contrast, seven genetically-identifiable populations of *E. similis* are present on MI suggesting that the different geological histories of the islands underlie the genetic diversity and that volcanism in combination with glaciation have been strong evolutionary drivers on MI.

Key words: Weevils, *Ectemnorhinus*, Marion Island, Prince Edward Island, COI gene, phylogenetics, biogeography, glaciation, volcanism, population dynamics, conservation

Introduction

Molecular phylogenies provide a valuable, unbiased evaluation of morphological-based classification of the *Ectemnorhinus* weevils (Grobler. *et al*., 2010a). In a recent study, Grobler *et al.* (2006) revealed that there was no genetic support for the existence of two distinct weevil species on Marion Island. As a result, *Ectemnorhinus similis* (Waterhouse, 1885) and *E. marioni* (Jeannel, 1940) were synonymised (Grobler *et al*. 2006; Chapter 2) and only one *Ectemnorhinus* weevil species, *E. similis* (Waterhouse, 1885), is presently recognised on Marion Island (MI), while two species, *E. similis* (Waterhouse, 1885) and *Ectemnorhinus kucheli* (Grobler, 2006) occur on Prince Edward Island (PEI). These results contrast markedly with what was originally expected as there was substantial support (Chown, 1990; Kuschel & Chown, 1995) for the presence of two size-discrete species, the larger *E. similis* (Waterhouse, 1885) and the smaller *E. marioni* (Jeannel, 1940) on MI. Due to the presence of weevils with the same morphology and body size classes on PEI, the presence of both species was inferred for this island, however, no formal taxonomic work had been performed on the weevils from PEI prior to the molecular study (Grobler *et al.* 2006), in which two possible reasons for the presence of just one species of *Ectemnorhinus* on MI were proposed, *viz*.: 1) There was originally two species of *Ectemnorhinus* present on MI, but that one of these species became locally extinct, possibly through body-size selective predation by mice (Chown & Smith 1993; Smith *et al.* 2002) and/or rapid climatic changes (Smith, 2002). Both factors could for example, remove the body size-induced reproductive barrier that was proposed on grounds of the significant relationship between female and male body size in *in-copula* pairs as observed by Chown (1990); or 2) That only one *Ectemnorhinus* species was ever present on MI and that the extreme morphological variation observed for *Ectemnorhinus* on the island was wrongly interpreted as indicating the presence of two species. Two possible reasons for the presence of two species of *Ectemnorhinus* on PEI were also proposed, *viz*.: 1) That because of the difference in glaciation histories, MI was extensively glaciated while PEI was not (Verwoerd, 1971), weevils on PEI may have had longer exposure to vascular plants as an additional, more nutritious food source to bryophytes than those on MI and may have diverged sympatrically according to the model of Rice (1984) into two species, a smaller one with a preference for bryophytes and a larger one with a preference for angiosperms, as suggested by Chown (1990); or 2) That the weevils on PEI and MI diverged from each other allopatrically resulting in an MI and PEI *Ectemnorhinus* species, with the subsequent

colonization of PEI by the MI *Ectemnorhinus* species, resulting in the presence of the two species seen on PEI today (Grobler *et al*., 2006).

In order to distinguish between these scenarios, a population-level study was undertaken in which genetic characterization of the COI gene of weevils sampled from across the islands, was performed. Both population genetics and biogeography were assessed in an attempt to gain insights into the complex and dynamic history of the *Ectemnorhinus* weevils occurring on the Prince Edward Islands archipelago (PEIA). Figure 1 shows the PEIA in the geographical context of the nearest land masses.

The results obtained in this study are in turn interpreted with reference to the geological history of the PEIA. Both MI and PEI are volcanic islands with MI being the tip of an active oceanic interplate volcano rising more than 3500 m from the ocean floor (Mahoney *et. al.*, 1992). The earliest sub-aerial eruptions occurred at least 450 000 years ago making MI at least 0.5 million years old (McDougall *et al*., 2001). The volcanic activity on MI is still active with recent eruptions being reported in 1980 (Verwoerd *et al.*, 1981) and 2004 (Meiklejohn & Hedding, 2005). Another small eruption consisting of gas only occurred in 2005 (I. Meiklejohn, pers. com.)

Hall (1981; 1982) suggested that MI went through three major glaciations while McDougall *et al*. (2001), on the basis of additional geo-chronological data, suggested that MI had at least five (possibly eight) different cold periods as well as eight different volcanic ages (Fig. 1) with some volcanic ages accompanying major glaciations (Fig. 2). Rapid deglaciation of MI at the end of the Last Glacial Maximum was proposed to have triggered the latest volcanic events (Hall, 1978; 1982; 2004). These so-called 'younger black lavas' have not been subjected to K-Ar dating as yet (McDougall *et al*., 2001). It was suggested that the rapid deglaciation of MI at the end of the Last Glacial Maximum started at 17-18 ka BP (Bianchi & Gersonde 2004). During the last glaciations, MI experienced a mean annual decrease in temperature of between 3º C and 6º C (Van Zinderen-Bakker, 1973; Hall, 1980; 1982) due to the fact that the Polar Front moved northwards to encompass MI and put the island within a zone of more southerly winds that were colder than those experienced at present (Hall, 1978). This drop in temperature initiated glaciation by causing the annual precipitation to fall in the form of snow rather than rain (Hall, 1978). As the glacier cover on MI was maintained by precipitation rather than by cold temperatures as is the case on Antarctica, a slight rise in temperature changed the precipitation back from snow to rain. The glaciers which were now cut off from their source in combination with higher temperatures led to rapid melting of the ice on MI despite the extensive cover (Hall, 1978). The lower possible limit of the palaeo-

snowline at maximum glacial conditions was 250 m and the upper was 550 m (Hall, 1978). Hall (1978) further hypothesised that the true snowline was most likely at 550 m. If this was true, it could maintain plant growth in unglaciated locations. The fact that plant life was not eradicated during glaciation, but that it survived in ice-free locations on MI has also been suggested by Van Zinderen-Bakker (1973) from pollen evidence. Hall (1978) further proposed that the snow cover was responsible for placing pressure on MI that resulted in the island being pushed under the water with a subsequent rise in sea levels of 3 m, 6 m and 10 to 11 m at different stages. The geological history of MI is summarised schematically in Figs. 3 and 4 in terms of volcanism and glaciation, respectively. It has been suggested that the Feldmark Plateau area on MI either remained ice-free through much of the last glacial maximum, or alternatively, the area was de-glaciated before other areas (Boelhouwers *et. al*., 2008). Boelhouwers *et. al*. (2008) also suggested that parts of Long Ridge may have remained ice-free during the Last Glacial Maximum.

Materials and methods

Genetic sampling

Ectemnorhinus weevil specimens were collected during three consecutive years (April 2001 – April 2003) from 30 localities encompassing the entire sub-Antarctic MI and from eight localities on PEI during April 2003 (see Appendix 1). All specimens were collected by hand and preserved in absolute ethanol.

Mitochondrial NA amplification and sequencing

DNA from each individual was extracted from a leg which, following removal from ethanol was washed and rehydrated in distilled water for 10 minutes prior to being frozen in liquid nitrogen and ground using a pestle. DNA was extracted using the High Pure PCR Template Preparation Kit from Roche Applied Science according to the supplier's procedure for isolation of nucleic acids from mammalian tissue. The only adaptation to the protocol was that the proteinase K digestion was performed for a minimum of 24 h instead of the 1 h digestion recommended for mammalian tissue by the supplier. MI-specific COI primers, GF-1858 and GR1-2938 (Grobler *et al*., 2006) were used to amplify a 1059 bp PCR product under the following reaction conditions: 200 ng of template DNA was added to 1×Buffer, 0.2 mM dNTP, 0.4 µM of each primer and 1 U *Taq* polymerase in a final volume of 50 µl. A

typical thermal cycling profile consisted of an initial denaturation step at 94º C for 90 s, followed by 40 cycles of 94º C for 22 s, 46º C for 30 s and 72º C for 1 min, and a final extension step of 1 min at 72º C.

Fig. 1 The Prince Edward Archipelago in the geographical context of the nearest land masses.

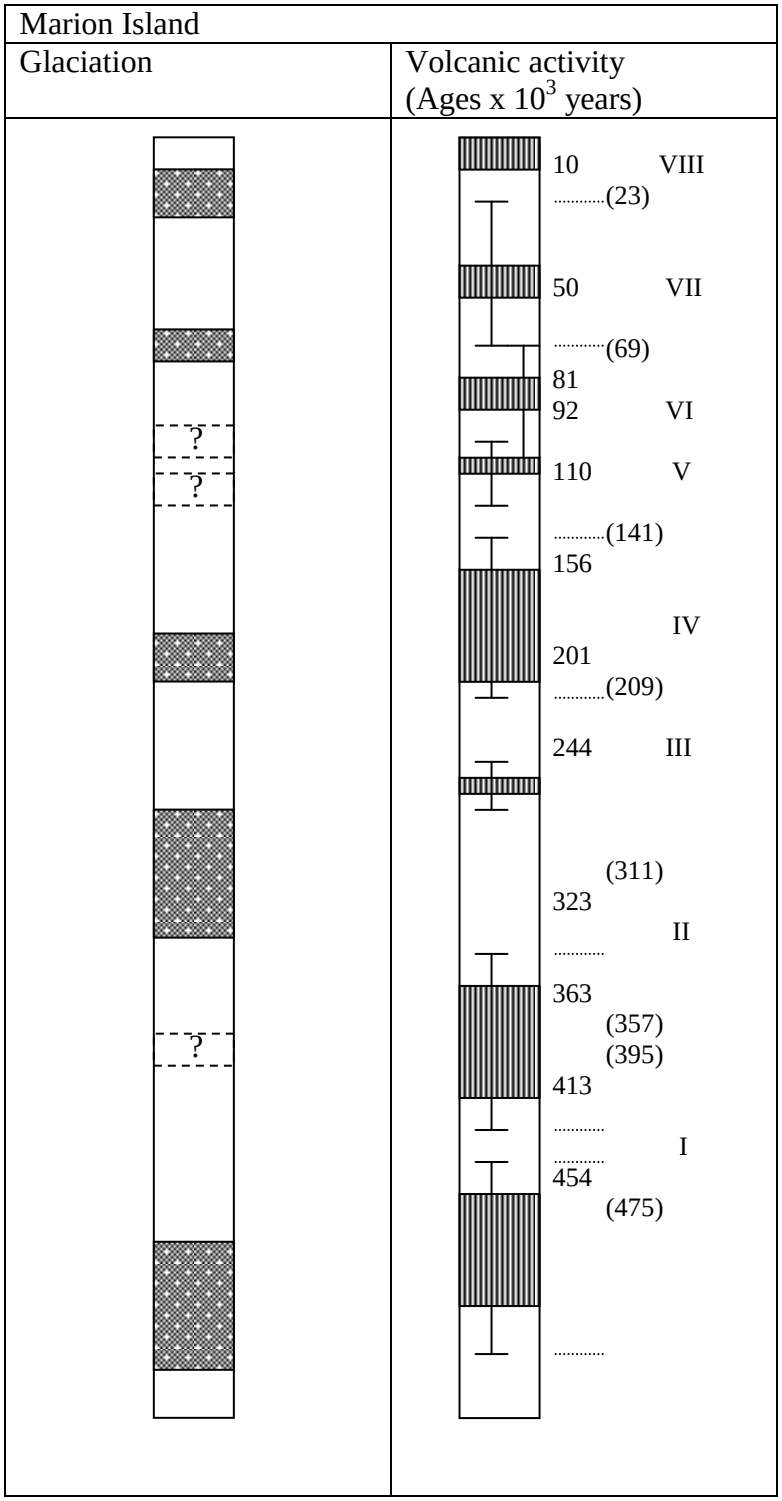

Fig. 2 Glacial and volcanic chronology from Marion Island (After McDougall *et al.,* 2001).

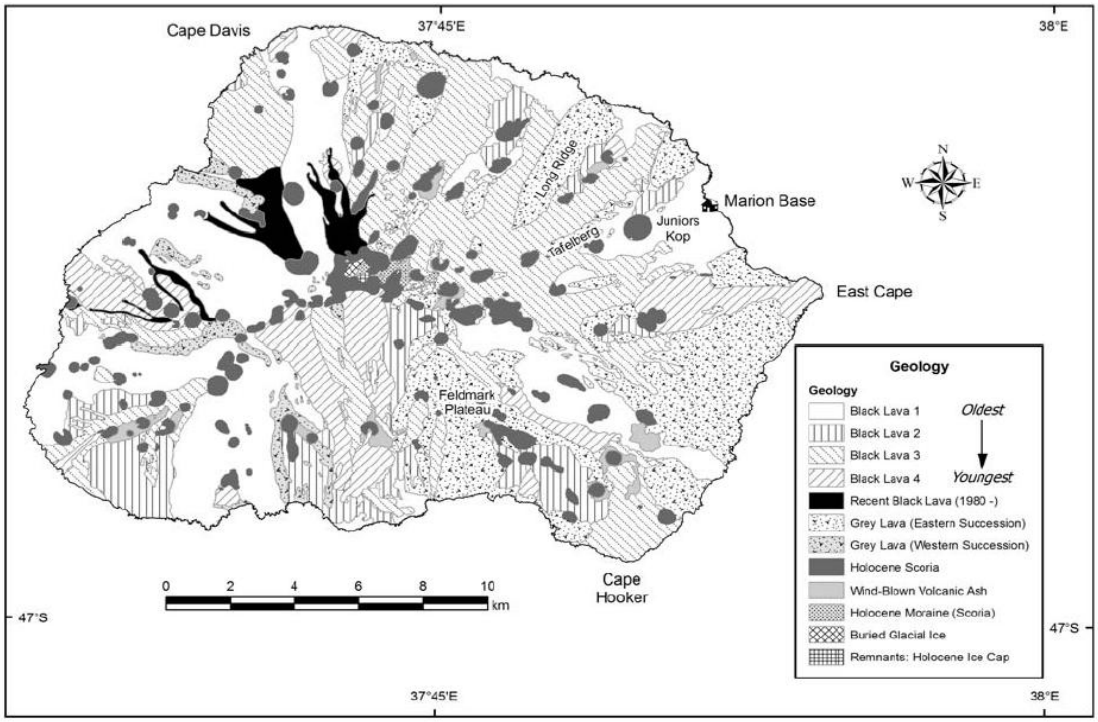

Fig. 3 Simplified geology of Marion Island (Modified after Verwoerd, 1971; Chevallier 1986; Chevallier *et al.*, 1992; McDougal *et al.*, 2001) as depicted in Boelhouwers *et al.* (2008).

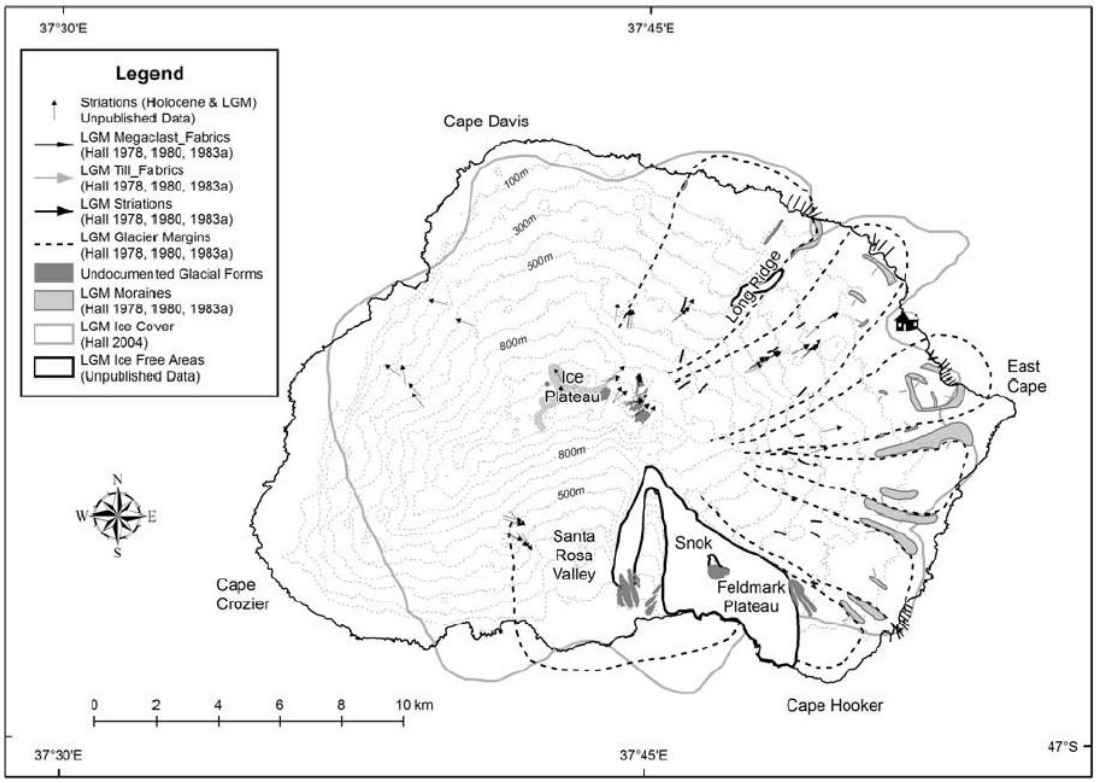

Fig. 4 Glacial margins, striae, and moraines as identified by Hall (1978) and a proposed local cirque near Snok as depicted in Boelhouwers *et al.* (2008).

The PCR product was purified directly from the tube using a Roche High Pure PCR Product Purification Kit. DNA sequences were determined by automated cycle sequencing on an ABI PRISM™ 3100 Analyser using the ABI PRISM Big Dye™ Terminator V3.0 sequencing standard. Primers GF5-1940 and GR5-2935 (Grobler *et al*., 2006) were used in all cycle-sequencing reactions following a thermal profile of 96º C for 10 s, 46º C for 8 s and 60º C for 4 min, repeated 25 times. The sequences were viewed and edited in Chromas 1.43 (McCarthy, 1996-1997) and aligned with DAPSA 4.9 (Harley, 2000).

Nested clade analyses

Although some criticism has been levelled against nested clade analyses (see Knowles & Maddison, 2002; Knowles, 2008), these concerns have been addressed (Templeton, 2008) and the method and its inferences remain valuable for understanding population dynamics. The program TCS 1.13 (Clement *et al*., 2000) was therefore used to generate a haplotype cladogram displaying the number of base pair differences between haplotypes. TCS 1.13 (Clement *et al*., 2000) incorporates the cladogram estimation algorithm described by Templeton *et al*. (1992) and provides 95 % parsimoniously plausible branch connections between the different haplotypes. Clades were nested by hand according to previously described nesting rules (Crandall, 1996; Templeton *et al*., 1987). Ambiguous connections were dealt with as outlined in Templeton & Sing (1993) as well as in Crandall & Templeton (1993). Geodis 2.0 (Posada *et al*., 2000) was used to test for significantly large and small clade (D_C) and nested clade (D_N) distances for clades and tip/interior contrasts when both genetic and geographical variations were present in the nested clade. D_C represents the mean distance between members of a clade and the geographical centre of that clade, providing an estimate of how geographically widespread the clade is. D_N represents the mean distance between the members of a particular clade and the geographical centre of all clades with which it has been grouped, including itself. This is a measure of the geographical isolation of a clade relative to the nested clade as a whole (Brown *et al*., 2002). Permutation analyses of all clades were based on 100 000 replicates in Geodis 2.0 (Posada *et al*., 2000). The inference key as obtained from http://darwin.uvigo.es/download/geodisKey_14Jul04.pdf was used to interpret the results obtained from Geodis 2.0 (Posada *et al*., 2000).

Phylogenetic analyses

jModelTest 0.1.1 (Posada, 2008; Guindon & Gascuel, 2003) was used to identify the model of evolution that best fits the data with parameters identified under the Akaike Information

Criterion (AIC; Akaike, 1974). The Minimum Evolution (Rzhetsky & Nei, 1992) algorithm in MEGA version 4 (Tamura et al. 2007) was used to construct phylogenies with node support assessed by 100 000 bootstrap replications. Minimum Evolution (Rzhetsky & Nei, 1992) trees were constructed using the Tamura-Nei (1993) distance correction algorithm and gamma distributions as estimated by jModelTest 0.1.1 (Posada, 2008; Guindon & Gascuel 2003). Bayesian phylogenetic analyses using MrBayes version 3.1.2 (Huelsenbeck & Ronquist, 2001) were performed on the complete dataset with the model and parameters recovered by jModelTest 0.1.1 (Posada, 2008; Guindon & Gascuel, 2003) being used to guide the setting of priors. The analyses were initiated with random starting trees and run for 10 000 000 generations with Markov chains sampled every 2000 generations. Of the 5000 trees obtained, 1250 were discarded as "burn-in". The equality of evolutionary rates between lineages was tested using the relative rate test (Li and Bousquet, 1992) in PHYLTEST version 2.0 (Kumar, 1996). In addition, the likelihood ratio test (Felsenstein, 1981; 1988) was performed, calculating and comparing log likelihood scores with and without the molecular clock enforced. A Neighbor Joining (NJ; Saitou and Nei, 1987) tree using uncorrelated p-distance values, with node support assessed by 100 000 bootstrap replications, was drawn in MEGA version 4 (Tamura *et al*., 2007) and divergence times were calculated from uncorrected pairwise values and calibrated using 2.3 % nucleotide sequence divergence per million years based on the arthropod mtDNA survey of Brower (1994). In addition, a BEAST analysis performed using BEAST 1.6.1 (Drummond & Rambaut, 2007) was used to obtain an ultrametric tree using Bayesian Monte Carlo Markov chain (MCMC) analysis orientated towards rooted, time-measured phylogenetics. Well-supported nodes identified following NJ, ME, ML and BI analyses were constrained to be monophyletic and divergence times were estimated using the 2.3 % nucleotide sequence divergence per million years, estimated from an arthropod mtDNA survey (Brower, 1994) and the appropriate parameter-rich model of evolution (Papadopoulou *et al*. 2010) selected under the AIC in jModelTest 0.1.1 (Posada, 2008; Guindon & Gascuel, 2003) using a strict molecular clock model. The results of two independent runs of 20 000 000 generations each with Markov chains sampled every 1000 generations, were merged and analyzed with Tracer v1.5 and TreeAnnotator v1.6.1 (Drummond & Rambaut, 2007). Of the 40 000 trees obtained, 5000 were discarded as "burn-in". Trees were rooted with *Ectemnorhinus viridis* (Waterhouse, 1853) from Heard Island since it has been shown to be closely related to the *Ectemnorhinus* weevils from the PEIA (Grobler et al. 2011a).

Mismatch analyses

Mismatch analysis provides information about demographic processes such as the magnitude and timing of population expansion based on the observed nucleotide pairwise distribution in the demographic mismatch analysis (Rogers & Harpending, 1992). It also characterizes the effect of range expansion independently of demographic expansion in the spatial mismatch analysis (Ray *et al*.. 2003; Excoffier, 2004). Pairwise mismatch distributions where the observed pairwise mismatch distributions were fitted to a stepwise expansion model by a generalized least square procedure as implemented in Arlequin version 3.5.1.2 (Excoffier & Lischer, 2010) were generated. The validity of a stepwise expansion model for the data was tested by MCMC simulations (1000 steps) with Arlequin version 3.5.1.2 (Excoffier & Lischer, 2010). A unimodal distribution is considered a signature of a population expansion, although it is not possible to establish whether it is a consequence of either demographic or spatial processes (Excoffier, 2004). A constant size population is expected to show a ragged, multimodal distribution, while an expanding population shows a smooth unimodal distribution. In each case, the raggedness index assesses the match of the real data to the model. A non-significant raggedness index indicates a relatively good fit of the data to a model of population expansion. The overall validity of the estimated expansion model was tested by comparing the distribution of the test statistic sum of squared differences (SSD), between the observed and the estimated mismatch distribution using a bootstrap approach. Evidence for departure from the estimated expansion model is given by significant SSD values. This can include either an expanding or a stationary population (Excoffier & Schneider, 1999). Population spatial expansion occurs if the range of a population is initially restricted to a very small area, and then the range of the population increases over time and over space. The resulting population becomes generally sub-divided in the sense that individuals will tend to mate with geographically close individuals rather than remote individuals. In the specific case of a range expansion, preferential reproduction with neighbouring individuals (local demes) should lead to some level of population structure while the local deme should nevertheless exhibit a unimodal mismatch distribution. Range expansion may thus produce the same genetic signature as a demographic expansion (Excoffier, 2004). The time of the main expansion in generations (t) was estimated from the equation $\tau = 2ut$ where $u = m_T\mu$ (m_T being the number of nucleotides used and μ being the mutation rate per generation) using the moment estimator of time to the expansion (τ) computed in Arlequin version 3.5.1.2 (Excoffier & Lischer, 2010) and a mutation rate of 2.3

% nucleotide sequence divergence per million years for arthropod mtDNA (Brower, 1994). As the weevils complete one generation in one-year (Chown & Scholtz, 1989), *t* could also be used as the time of the main expansion in years. Thus $t = \tau / 2(0.000000023 \times 885 \times 1) = \tau / 0.00004071$. For the spatial expansion the tree parameters τ, $\theta = \theta_0 = \theta_1$ (assuming that $N = N_0$), and $M = 2Nm$ were estimated and the rate at which the sampled deme would exchange migrants with a unique population of infinite size (m) was calculated. The analysis of spatial mismatch, based on the assumption of no demographic expansion within the sampled deme, provides an estimate ($N_f = \theta/2u$) of the effective female population size necessary to explain the mismatch distribution uniquely in terms of range expansion (Excoffier, 2004). Thus $N_f = \theta/2(0.000000023 \times 885 \times 1) = \theta/0.00004071$. Arlequin version 3.5.1.2 (Excoffier & Lischer 2010) was utilized to carry out Fu's (1997) F_S test of neutrality as well as to estimate Tajima's *D* and the essential population parameter θ (Tajima 1983).

Statistical analyses

Haplotype diversity (h) and nucleotide diversity (π) were estimated in DNASP 5.1 (Librado & Rozas, 2009). π is the average number of nucleotide differences between two sequences from one population (Nei & Li, 1979). Genetic structure was investigated with Arlequin version 3.5.1.2 (Excoffier & Lischer, 2010) as well as with DNASP 5.1 (Librado & Rozas 2009). Genetic structure analyses include F_{ST} values (fixation indexes), N_{ST} values as well as the number of migrants per generation. N_{ST} (Lynch & Crease, 1990) is almost the same as F_{ST} (Hudson *et al*., 1992), except that for N_{ST}, the correction of Jukes & Cantor (1969) has been applied. The larger the F_{ST} / N_{ST} values the larger the genetic variation between the sub-populations in terms of the total population (Holsinger & Weir, 2009). The average number of pairwise differences between populations (Pi_{XY}), the average number of pairwise differences within each population (Pi_X) as well as the corrected average pairwise difference between populations (Pi_{XY}-(Pi_X+Pi_Y)/2) were also calculated using Arlequin version 3.5.1.2 (Excoffier & Lischer, 2010). Analysis of molecular variance (AMOVA; Excoffier *et al.*, 1992) was utilised to investigate the population structure by calculating the among-population and within-population variation when assessing all individuals sequenced (Excoffier & Lischer, 2010). An overall fixation index was also uncovered by the AMOVA analysis which was performed using Arlequin version 3.5.1.2 (Excoffier & Lischer, 2010). Divergence times (tau) allowing for unequal population sizes between genetically distinct clades was also calculated using Arlequin version 3.5.1.2 (Excoffier & Lischer, 2010) .

Discussion

Phylogeography

In order to gain insights into the patterns of the *Ectemnorhinus* population dynamics on the PEIA it is important to first consider the results of both the nested clade analyses as well as the phylogenetic analyses. These results are also meaningful if interpreted in context of Figs. 9–14 where the haplotype network was superimposed on the island maps according to sampling localities. As a single haplotype network was obtained, it allowed the evaluation of each sample relative to the rest.

In Fig. 12, the individuals that form nested clade 4-4 (Figs. 6 & 8) are mapped according to their sampling localities. All the individuals of nested clade 4-4 map to PEI and the individuals in this clade have been designated *E. kucheli* (Grobler *et al*., 2006). This clade has also been designated the base of the nested clade analyses (Figs. 6–8) as it has been shown to be older than the other clades (Grobler *et al*., 2006). In this study, nested clade 4-4 was found to be the most basal clade in the Bayesian tree with all other clades grouping together with 92% support (Fig. 16). Of all the nested clades for which time to lineage

coalescence was calculated, nested clade 4-4 gave the oldest time of approximately between 0.312 MYA (Fig. 17) and 0.5109 MYA (Fig. 18), indicating that it was the first to have colonised the PEIA. The Tau values (Table 15) indicate that in each case, the pairwise divergence times from nested clade 4-4 are the oldest. These results provide support for the decision to use nested clade 4-4 as the most basal clade in the nested clade analyses. Although nested clade 3-10 was one of the few nested clades that showed a significant relationship between genetic variation and the respective geographical locations of the haplotypes (Table 1), the nested clade analyses could not provide a conclusive outcome (Table 2). However, when the individuals of nested clade 4-4 were mapped according to sampling locality, it was evident that the whole sampling area on PEI was represented (Fig. 12a). Even the four haplotypes that have more than one representative span large areas of the sampling transect (Fig. 12b). When we consider Figs. 12c–f and compare it to the PEI volcanological map (Fig. 3) it is possible that the younger Holocene black basaltic lavas were colonised from the older Pleistocene grey lavas to the northeast. It is interesting to note that individual 17-14, collected from the Golden Gate area, is separated from the remainder of nested clade 4-4 individuals by eight steps / missing haplotypes (Fig. 6).This individual is possibly a representative of a population that was isolated by the younger black lavas east of Karterkoppie from other con-specifics inhabiting the older grey lavas (Fig. 3). Individual 17-14 appears to represent a discrete sub-population of *E. kucheli* on PEI that is less abundant than the main population.

As *E. kucheli* was the first species to colonise the PEIA at PEI, Grobler *et al.* (2006) suggested that the presence of *E. similis* on MI could perhaps be explained by the initial colonisation of MI by PEI *E. kucheli* followed by differentiation into a new species *E. similis* and the extinction of the ancient colonisers.

In so far as the population dynamics of *E. similis* on MI is concerned, nested clade 4-4 is only connected with nested clade 4-5 (Figs. 6– 8). This suggests that the individuals within nested clade 4-5 are the closest relatives to the original migrants to MI. The phylogenetic analyses (Figs. 15 & 16) show that nested clade 4-5 separates into two distinct clades, clade 4-5a & 4-5b. Although both clades have less than 50 % bootstrap support in the ME analyses (Fig. 15), clade 4-5a has 94 % support in the Bayesian analyses, while clade 4-5b has 85 % support (Fig. 16). Both clades form monophyletic groups within *E. similis* in the Bayesian analyses (Fig. 17). With no significant support for any of the internal nodes, the ME analyses (Fig. 15) provide no indication of the internal structuring of the clades. The nested design shows that clade 4-5b separates from clade 4-5a as clade 4-5b is enveloped in nested clade 3-

2 (Figs. 6 & 8), the individuals in clade 4-5a separated from those in clade 4-5b by six and eight missing haplotypes (Fig. 6). The time of lineage coalescence of clades 4-5a and 4-5b indicate that clade 4-5a arose between 0.193 MYA (Fig. 17) and 0.3206 MYA (Fig. 18), while clade 4-5b arose approximately between 0.216 MYA (Fig. 17) and 0.226 MYA. Clade 4-5a is also the second oldest clade according to the BEAST analyses (Fig. 18) making it the oldest on MI and indicating it as the original colonizer of MI from PEI. In Fig. 17, clade 4-5b appears to be older than clade 4-5a. The examination of both in the nested design (Fig. 6) indicates that there are seven missing haplotypes between members of clade 4-5b (nested clade 3-2). This very high number of missing haplotypes between members of the same clade may considerably distort the evolutionary scenario given that more complex population dynamics may be playing a role. It is thus plausible to assume that clade 4-5a was the original *E. similis* on MI. It is possible that clade 4-5b diverged from clade 4-5a and this is discussed in greater detail below.

Three of the eight nested clades that showed significant relationships between genetic variation and the respective geographical locations of the haplotypes (Table 1) fall within nested clade 4-5. In Fig. 13 where the sampling localities of all the individuals that form part of nested clade 4-5 have been mapped, it was found that they all map to MI with no representatives on PEI (Fig. 13a). In Fig. 13b, the eight haplotypes that consist of more than one representative have been indicated. H5 and H24 can be identified as two major haplotypes (Fig. 6). H5 consists of nine individuals of which three were collected from Swartkop. The remaining individuals that form part of H5 were either sampled at the coast or near to it, both in a northern and southern to western direction (Fig. 13b). H24 consists of ten individuals and forms a similar path around MI as H5 except that H5 seems to be distributed more widely distributed across the bottom of the eastern escarpment while H24 occurs across the top of the eastern escarpment (Fig. 13a). Although H5 and H24 are both part of clade 4-5a (Fig. 15 and Fig 16) it seems that they were at least partially divided by the shear steepness of the eastern escarpment. The other haplotypes that have more than one representative map primarily to the western side of MI, with the exception of H2 that is also located at Swartkop and H10 that forms part of clade 4-5b (Figs. 15 & 16). At the 1-step level (Figs. 6, 8 & 13c), nested clade 1-96 represents one of the nested clades that have a significant relationship between its genetic variation and the respective geographical locations of its haplotypes at the 0.05 % level of significance (Table 1). Table 2 indicates restricted gene flow / dispersal, with some long distance dispersal, as a likely explanation. At the 2-step level (Fig. 13d), nested clade 2-18 shows a significant relationship between genetic variation and geographical

locations of its haplotypes at the 0.1 % level of significance (Table 1) consistent with continuous range expansion (Table 2). The tracing of the nested succession through to Fig. 13e shows that all the individuals in nested clade 4-5 can be divided into three 3-step nested clades (Figs. 6, 8 & 13e). Of the 3-step nested clades, nested clades 3-16 and 3-6 form part of clade 4-5a (Figs. 15 & 16) while nested clade 3-2 correlates with clade 4-5b (Figs. 15 & 16). Both nested clades 3-16 and 3-6 appear to form a ring around the island. The map of the glacial history of MI (Fig. 4) indicates that the south-western part of the island was not glaciated during the last glacial maximum and that this ice-free area occurred below as well as above the western escarpment. The remainder of MI was completely covered in ice, except for two possible sites at Feldmark Plateau and Long Ridge (Fig. 4). At the end of the last glacial maximum, the ice cover on MI contracted and the coastal areas became exposed first. It is likely that the extensive ice coverage during the last glacial maximum, all weevils on MI except those on the south western side of the island, succumbed. As the ice melted, the coastal areas became exposed and available for re-colonisation by plants as well as weevils. From this initial re-colonisation it appears that the weevils moved in both a westerly and easterly direction along the coast, recolonising the remainder of the island with the help of the strong, frequent winds from the SW, as opposed to the weaker infrequent winds from the NE (Schulze, 1971). Early Holocene post-glacial volcanism (Hall, 1978; 1982; 2004) may also have provided the impetus for weevil migration from the south-western side of the island to other available habitats in the east and north. The population that survived the glaciation in the south-western corner of the island also survived the extensive post-glacial volcanism of this region with the ancestors of nested clade 3-16 being protected at Coldridge and the ancestors of nested clade 3-6 being protected at the Pyroxene Kop area (Fig. 3). The fact that MI rises 1280 m above sea level (Langenegger & Verwoerd, 1971) and that large parts of the higher altitudes were still mostly under ice until recent years (Sumner *et al.*, 2004) explains the west-east lower-altitude movement of weevils around the island rather than traversing the high altitude section of the island. Although not traversed, some higher altitudes sites were colonised by the weevils from clade 4-5a again most likely with the assistance of the strong, frequent south-westerly winds (Schulze, 1971). The large degree of 3rd-stage Holocene post-glacial volcanism to the north and east would have hampered re-colonisation from the north-eastern and eastern sides of MI (Fig. 3).

Clade 4-5b does not group with clade 4-5a in the phylogenetic analyses (Figs. 15 & 16) although the nested analyses (Fig. 6) show that it links only with the individuals from clade 4-5a and was also included in nested clade 4-5. Fig. 13e shows that clade 4-5b (nested

clade 3-2) seems to have been isolated in the northern part of the island from the rest of nested clade 4-5 and spread from there to the south and east. The ancestors of the weevils that today comprise clade 4-5b may have emanated from the weevils that were isolated in the south-western corner of MI as the ice cover began to retract. Holocene post-glacial volcanism (Hall, 1978; 1982; 2004) in this area may then have isolated the migrants on this part of the island into a small population (Fig. 3), allowing it only to expand to the rest of the island after the black lavas became hospitable. The only evidence for the expansion of this population in this study is in an eastern direction that again correlates with the strong, frequent south-westerly winds (Schulze, 1971). Nested clade 4-5 (Figs. 6, 8 & 13f,) shows a significant relationships between its genetic variation and the respective geographical locations of its haplotypes at the 0.05 % level of significance (Table 1) although the nested clade analyses showed no conclusive evidence for this (Table 2). This may be due to the close proximity of the sampling localities.

Clade 4-6 forms a monophyletic clade in both phylogenetic analyses with less than 50 % bootstrap support in the ME tree (Fig. 15) and 93 % support in the Bayesian tree (Fig. 16). The monophyletic status of this clade is also confirmed by the nested clade analyses where the individuals nesting in nested clade 4-6 are separated by three missing haplotyes from nested clade 4-5 and by 7 missing haplotypes from nested clade 4-1 (Figs. 6 & 7). No significant relationships between the genetic variation and the respective geographical locations of the haplotypes were shown for any of the nested clades (Table 1). Examination of the distribution and subsequent relationship between the individuals on the maps (Fig. 14), reveals only a single haplotype with more than one representative (Fig. 14b). It is possible that clade 4-6 may have been part of the weevils that migrated west-wards from the south-westerly glaciations-isolated clade 4-5a after the ice retracted. The most probable explanation is that it was isolated from the rest of the weevils in the Sidney area as the area to the south of Sidney was sheltered from the lava from the Holocene post-glacial volcanism (Fig. 3). Its small population size explains the low number of specimens collected. When the lava became hospitable again this population expanded north-wards (Fig. 14) and probably also west-wards with the aid of the strong, frequent south-westerly winds (Schulze, 1971). However, no samples were collected west of Sidney to substantiate this and it is also possible that a large amount of younger lava flow in the Santa Rosa area would have impeded a west-ward migration (Fig. 3).

Figs. 6 & 7 show that nested clade 4-1 is more closely connected to nested clade 4-6 than to any other clade. Although none of the clades nested within nested clade 4-1 show any

significant geographical association (Table 1), when individuals comprising nested clade 4-1 (Figs. 3 & 5) are mapped according to their sampling localities (Fig. 9a), the MI portion of samples map mainly to the eastern side of MI and the PEI portion of the samples are distributed along almost the whole of the gradient sampled. Nested clade 4-1 forms a monophyletic clade in both phylogenetic analyses with 83 % bootstrap support in the ME tree (Fig. 15) and 100 % support in the Bayesian tree (Fig. 16). The monophyletic status of this clade is also confirmed by the nested clade analyses where the individuals nesting in nested clade 4-1 are separated from the rest of haplotype network by seven missing haplotypes from the split with clade 4-6 (Figs. 6 & 7). Fig. 9b shows that three sets of identical haplotypes within the nested clade 4-1: H4 that has two individuals from Tate's Hill and one individual from Stony Ridge, H125 that links the MI meteorological base at Transvaal Cove with Stony ridge and H66 that forms a link between Halfway Kop on MI with PEI. The tracing of the nested diagram further through Fig. 9c – 9e shows its development into two 3-step nested clades. Nested clade 3-8 consists of eight individuals that all come from Stony Ridge and Tate's Hill. Nested clade 3-9 on the other hand, is geographically not as well structured. Nested clade 3-9 at the lower levels shows that it consists of three 2-step nested clades (Fig. 9d). Nested clade 2-4 consists of two individuals connecting the Albatross Lakes area of MI with PEI, nested clade 2-3 consists of eight individuals connecting Halfway Kop with Jonny's Hill, Kildalkey Bay, Tate's Hill as well as the rest of the individuals from PEI and nested clade 2-34 that consists of nine individuals that connects Transvaal Cove with Junior's Kop, Repetto's Hill, Tate's Hill, Kildalkey Bay and Watertunnel. Past geographic events in this region suggest that the whole eastern region, with the possible exception of the Feldmark Plateau area, was covered in ice during the last glacial maximum (Fig. 4). When the ice retracted, the coastal parts of MI were available for re-colonization by weevils from the western side of the island. First stage Holocene post-glacial volcanism (Hall, 1978; 1982; 2004) that covered the area south of Skua Ridge to the north of Macaroni Bay as well as south of Kerguelen Rise (Fig. 3) may have been responsible for the isolation of the population that is currently found in nested clade 4-1 (Fig. 9f). Subsequent Holocene post-glacial volcanism (Hall, 1978; 1982; 2004) likely underlies the formation of the different 3-step nested clades shown in Fig. 9e. Individuals from nested clade 3-8 were isolated at the Tate's Hill - Stony Ridge area by the 3rd- and 4th-stage Holocene post-glacial black lava (Fig. 3) from the individuals in nested clade 3-9. A question that arises is why no individuals of nested clade 4-1 occur to the west and only a few to the north? Western migration may have been prevented firstly by the 3rd- and 4th-stage Holocene post-glacial black lava that links

Green Hill with Johnny's Hill and north-west from there as well as the extensive 3rd- and 4th-stage Holocene post-glacial black lava in the Santa Rosa valley (Fig. 3). North-ward expansion was most possibly hampered firstly by the 1st-stage Holocene post-glacial black lava that covers the whole area south of Skua Ridge to the north of Macaroni Bay, and secondly by the subsequent 3rd- and 4th-stage Holocene post-glacial black lava that extends west-wards from East Cape as well as the other more extensive 3rd-stage Holocene post-glacial black lava to the north (Fig. 3).

The nested design (Fig. 6) shows that nested clade 4-3 has connections with both nested clade 4-5 and nested clade 4-1. There are nine missing haplotypes between nested clade 4-3 and nested clade 4-5 and 12 missing haplotypes between nested clade 4-3 and nested clade 4-1. The fact that nested clade 4-3 connects with both nested clade 4-5 and nested clade 4-1 suggests that it separated from both at some stage in the past. The individuals that comprise nested clade 4-3 group together as clade 4-3 in the ME analyses (Fig. 15), with 91 % bootstrap support, as well as in the Bayesian analyses (Fig. 16), with 100 % support. In both the ME analyses (Fig. 15) and the Bayesian analyses (Fig. 16) some internal nodes with high support are present. Although none of the clades nested within nested clade 4-3 show any significant geographical association (Table 1), when the individuals that form part of nested clade 4-3 were mapped according to their sampling localities, the MI portion of samples map mainly to the north-eastern side of MI (Fig. 11a). Clade 4-3 also has some representatives on PEI although none of the samples collected from the higher altitudes on PEI fall into this group. When the haplotypes containing more than one representative were included (Fig. 11b), five different groupings were revealed. Of these groupings, H34 with 12 different representatives is the most prominent. One of these haplotypes connects the weevils from MI to the weevils from PEI. The tracing of nested design from Fig. 11c to 11f and its comparison to the geographical history of the area with reference to the volcanological map of MI (Fig. 3) shows that the north-eastern side of MI is very fractured by Holocene post-glacial black lavas from all four stages. The same boundary that hampered the north-wards spread of nested clade 4-1, namely the 1st-stage Holocene post-glacial black lava that covers the whole area south of Skua Ridge to the north of Macaroni Bay (Fig. 3) as well as the subsequent 3rd- and 4th-stage Holocene post-glacial black lava extending west-wards from East Cape (Fig. 3) also seems to have restricted the south-ward movement of individuals of nested clade 4-3. The northern migration of individuals from nested clade 4-1 (Fig. 9a) might have been aided by the strong, frequent south-westerly winds (Schulze, 1971) while the southern migration of individuals from

nested clade 4-3 (Fig. 11a) might have been hampered by the strong, frequent south-westerly winds (Schulze, 1971). The east-ward migration of nested clade 4-3 may have been hampered firstly by the 3rd-stage Holocene post-glacial black lava found between Ned's Kop and the north of Ship's Cove (Fig. 3) and further by the 3rd-stage Holocene post-glacial black lavas west of Long Ridge and those east of Repetto's Hill (Fig. 3). The fact that clade 4-3 has so many internal clades with high support (Figs. 15 & 16) may be due to the north-eastern side of MI being very fractured by Holocene post-glacial black lavas from all four stages. This may have resulted in fragmentation of the original population that groups into clade 4-3 (Figs. 15 & Fig. 16) into small isolated pockets that started to diverge from each other. The original boundaries of these small isolated pockets may have been formed by the 1st-stage Holocene post-glacial black lavas (Fig. 3), but are at present obscured by the subsequent Holocene post-glacial black lavas (Fig. 3). The older grey basaltic lavas that can be observed at present, as well as northeast of, Tafelberg may be possible sites for their survival during the 1st-stage Holocene post-glacial black lavas (Fig. 3).

The individuals that form part of nested clade 4-2 in the phylogenetic analyses are, in both the ME analyses (Fig. 15) and the Bayesian analyses (Fig. 16), divided into two different clades, namely, clade 4-2a and 4-2b. Both clades have high support in both phylogenetic analyses (Figs. 15 & 16). Nested clade 4-2 in the nested design (Fig. 6) shows that there are seven missing haplotypes between nested clade 1-56 that corresponds to clade 4-2b, and nested clade 3-4 that corresponds to clade 4-2a. Noteworthy is that there are also seven missing haplotypes between some of the individuals within clade 4-2a and nested clade 3-4 (Fig. 6). Nested clade 4-2 is also one of the clades that show a significant relationship between its genetic variation and the respective geographical locations of its haplotypes at the 0.1 % level of significance (Table 1). The nested clade analyses suggest allopatric fragmentation for this relationship (Table 2). Fig. 10, where the individuals from nested clade 4-2 were mapped according to their sampling localities, show that all the individuals that belong to clade 4-2b map to MI while those that belong to clade 4-2a map to PEI and that they are so divided up to the 3-step level (Fig. 10a–e). Allopatric fragmentation as suggested by the nested clade analyses (Table 2) is thus evident. No conclusions can be drawn from the ME tree as to the relationship between clade 4-2a and clade 4-2b with the rest of the clades, due to lack of support for the internal nodes (Fig. 15). Nonetheless, the Bayesian analyses (Fig. 16) show that both clade 4-2a and clade 4-2b group within *E. similis* rather than with *E. kucheli* and the nested design (Fig. 6) shows that nested clade 4-2 only has ties with nested clade 4-5 and none with nested clade 4-4, strongly suggesting an MI rather than a PEI origin.

Patterns of mtDNA variation

All methods of calculating F_{ST} values (Tables 10 & Table 11) gave very high F_{ST} values for all the pairwise comparisons when they were calculated among the different clades as identified in Figs. 15 and 16. The number of migrants between these clades is also in each case less than one migrant per generation (Table 10). Similar results were obtained from the N_{ST} values (Table 12). From Table 14, the among-clade variation was 2.71 times higher than the within-clade variation, while the fixation index is also very high being above 70 %. These results suggest that the isolation of the different clades, as discussed previously, was sufficiently to prevent viable gene flow between clades. The first major isolation was when MI was colonised from PEI. This separation by distance and the ensuing allopatric speciation resulted in the emergence of *E. kucheli* on PEI and *E. similis* on MI. The last glacial maximum as well as the subsequent Holocene post-glacial volcanism was responsible for pocketing the *E. similis* weevils on MI in small populations that correspond to the different clades that are currently present on the island. In light of the evidence provided by the F_{ST} values, it is suggested that the separation of the original populations occurred to such an extent and for sufficient time that they diverged into the different populations that are currently detectable. Athough they presently have a sympatric distribution, the distinct genetic signature has been retained and there is no noticeable gene flow between them.

Population expansion

Clear indications for population growth were supported by several lines of evidence, including genetic diversity statistics, mismatch analyses and neutrality tests for *E. kucheli* on PEI as well as for all the genetically-identifiable populations of *E. similis* on MI. For all groups, the nucleotide diversity was relatively low and the haplotype diversity was extremely high (Table 9), suggesting a population expansion. The neutrality tests also show strong support for population expansion of *E. kucheli* on PEI as well as for each of the genetically-identifiable populations of *E. similis* on MI. Instances where a weak signal was obtained, eg. clades 4-2a and clade 4-5b, are likely attributable to small sample sizes and the large numbers of missing haplotypes. Further evidence for both demographic expansions and range expansions were obtained from the mismatch analyses (Tables 6 & 7) and in each case, except in the cases of clades 4-2b and 4-6, demographic expansions predates range expansions. This makes sense in the light of the geographical history as major expansion was necessary for each genetically-identifiable population to cover its present geographical range after its original isolation by the Holocene post-glacial volcanism.

Conclusions

The present study suggests that PEI was the first of the two islands of the PEIA to be colonized by *Ectemnorhinus* weevils, and a time of coalescence of approximately 0.312 MYA (Fig. 17) and 0.5109 MYA (Fig. 18) was estimated for this event. No evidence of glaciation was found on PEI. If indeed PEI was not glaciated, it may explain the survival of *Ectemnorhinus* weevils through the glaciation stages suggested by McDougall *et al.* (2001) as indicated in Fig. 1a. The PEI population then acted as the source population for the colonization of MI by *Ectemnorhinus* weevils some time before the last glaciation, approximately 10 000 to 35 000 years ago (Fig. 2). This would give the weevils an approximate maximum of 30 000 years, the amount of time between the last glaciation and the one before, to colonize the whole of MI (Fig. 2). The current data suggest that strong, frequent winds from the SW as opposed to the weaker infrequent winds from the NE (Schulze, 1971) hampered the movement of weevils from east to west. Sufficient time for this east-west movement was thus available. The separation by distance of the PEI *Ectemnorhinus* weevils from those on MI then gave rise to two species by allopatric speciation, namely *E. kucheli* on PEI and *E. similis* on MI. During the last glaciation MI was extensively glaciated with only the south-western corner of the island being ice-free (Fig. 4). The extensive glaciation of MI may have resulted in the extinction of *E. similis* on MI except for the populations occurring on the ice-free south-western corner of the island. The weevils that at present group in clade 4-5 (Figs. 15 & 16) appear to be represent the relict population of the original MI colonizers that were able to migrate, despite the resistance of the strong, frequent south-western winds (Schulze, 1971), to the south-western corner of MI. This may also explain why clade 4-5 is the MI clade that is most closely related to *E. kucheli* on PEI (Table 15) despite the presence of geographically closer clades on the eastern side of MI. Date estimates obtained by the molecular clock should always be interpreted with caution as it is a subject of considerable debate (Graur & Martin, 2004). In this case, it is even more so as the time of coalescence for the individuals that comprise clade 4-5a was calculated from weevils that firstly originated from PEI. If the current observation of very high numbers of unique haplotypes in each clade is taken into account, the same trend may most possibly have been the case on MI before the last glaciation. Estimates from the Bayesian analyses may be over-inflated due to insufficient time for fixation of mutations. At the end of the last glacial maximum, when the ice started to melt, the coastal areas of MI emerged first from beneath the ice and were available for the re-colonization by the weevils. The movements of the weevils that were isolated in the south-western corner of MI, along the coastal areas of the

island, may have been assisted by the strong, frequent south-westerly winds (Schulze, 1971), and may have occurred over a very short time span. Evidence for this short time span comes from the observation that weevils that are members of clade 4-5 are currently found over the entire MI. Subsequent Holocene post-glacial volcanism (Hall, 1978; 1982; 2004) was then responsible for the fragmentation of the new migrants, resulting in small pockets of weevils across the island, surrounded by fresh, uninhabitable lava. As with the weevils that were isolated in the south-western corner of MI by the ice, these pockets of weevils, isolated by the lava, were not necessarily very closely related. The main pockets of isolated weevils correlate with the different clades that are identifiable at present: clade 4-5b that was isolated in the north of MI in the Cape Davis area, clade 4-3 that was isolated in the extensively fragmented north-east of MI, clade 4-1 that was isolated in the east of MI in the Tate's Hill – Stony Ridge area, clade 4-5 was again isolated by the lava in the south-western side of the island, clade 4-6 that was isolated in the Sidney Hill area and clade 4-2b that consists of a very small population of which sample size in the present study is too small for valid conclusions. The time it took for the different populations of isolated weevils to recover from the devastation of the lava as well as the time it took for the lava that isolated the weevils in small populations to become inhabitable for re-colonization by weevils was sufficient for the weevils in each population to diverge from those in the other populations. When the Holocene black lavas became re-colonizeable, the weevils from the different isolated populations may have again migrated to the rest of the island. The population that in the present study was recognised as clade 4-5a may again have spread over the entire MI with the assistance of the strong, frequent south-westerly winds (Schulze, 1971). The population that in the present study was denoted clade 4-1 was hampered by the strong, frequent south-westerly winds (Schulze, 1971) in their south-ward and west-ward migration but were much freer to disperse to the north. The 3rd- and 4th-stage Holocene post-glacial black lava (Fig. 3) may to some extent also have hampered both the east-ward and the north-ward migration of this population. The population that was recognised as clade 4-3 in the present study, like clade 4-1, was hampered by the strong, frequent south-westerly winds (Schulze, 1971) in their south-ward migration. Both west-ward and south-ward migration may also have been hampered by 3rd- and 4th-stage Holocene post-glacial black lava (Fig. 3). The population that was recognised as clade 4-6 in the present study was a very small population, and its east-ward migration may most likely have been blocked by the 3rd- and 4th-stage Holocene post-glacial black lava at Santa Rosa valley (Fig. 3). Only north-ward migration was thus possible for members of this population. The strong, frequent south-westerly winds (Schulze, 1971) as

well as the large amount of 3rdstage Holocene post-glacial black lava north of Triegaardt Bay may have prevented the westward movement of individuals from the population that was recognised as clade 4-5a in the present study. Currently, members of the different genetically-identifiable populations occur sympatrically, and in some cases even on the same plant, but with no noticeable geneflow being detected between them. It is thus suggested that the time of isolation, before the Holocene post-glacial black lavas became hospitable was sufficiently long and the populations sufficiently small that a number of genetically-discrete populations arose. The present study recognised two discrete populations of *E. kucheli* on PEI and seven of *E. similis* on MI. The fact that the living conditions and food available for all the different isolated populations were identical may explain why members of the different genetically-discrete populations are morphologically indistinct. It is suggested that breeding experiments between individuals from the different genetically-discrete populations should be undertaken to determine whether they are able to interbreed and if not, to determine whether there are some external factor(s) that may be preventing geneflow between them. This study supports Grobler *et al*. (2011b) who emphasized the need for the prevention of anthropogenic geneflow between MI and PEI in order to not interfere with the natural population dynamics. The current practice of limiting visits to PEI should be maintained as well as the strict provisions for quarantine for such visits. The presence of numerous genetically-discrete populations of *E. similis* on MI that do not occur on Prince Edward Island and that are under threat via increased size-selective predation by the house mouse, *Mus musculus domesticus* (Chown & Smith, 1993), underscores the urgency for control of mice on Marion Island before these genetically-discrete populations become extinct.

References

Akaike, H. 1974. A new look at the statistical model identification. *IEEE Transactions on Automatic Control* 19:716-723.

Bianchi, C. & Gersonde, R. 2004. Climate evolution at the last deglaciation: the role of the Southern Ocean. *Earth and Planetary Science Letters* 228: 407-424.

Boelhouwers, J., Meiklejohn, I., Holness, S. & Hedding, D. 2008. Geology, geomorphology and climate change. *In* Chown, S.L. & Froneman, P.W. *eds. The Prince Edward Islands. Land-Sea Interactions in a Changing Ecosystem*. African Sun Media, Stellenbosch, 65-96.

Brower, A.V.Z. 1994. Rapid morphological radiation and convergence among races of the butterfly *Heliconius erato* inferred from patterns of mitochondrial DNA evolution. *Proceedings of the National Academy of Sciences of the United States of America* 91: 6491-6495.

Brown, R.P., Suárez, N.M. & Pestano J. 2002. The Atlas mountains as a biogeographical divide in North-West Africa: evidence from mtDNA evolution in the Agamid lizard *Agama impalearis*. *Molecular Phylogenetics and Evolution* 24: 324-332.

Chevallier, L. 1986. Tectonics of Marion and Prince Edward Volcanoes (Indian Ocean): results of regional control and edifice dynamics. *Tectonophysics* 124: 155-175.

Chevallier, L., Verwoerd, W.J., Bova, P., Stettler, E., du Plessis, A., du Plessis, J.G., Fernandez, L.M. & Nel, M. 1992. Volcanological features and preliminary geophysical investigations on Marion Island. *South African Journal of Antarctic Research* 22: 15-35.

Chown, S.L. 1990. Speciation in the sub-Antartica weevil genus *Dusmoecetes* Jeannel (Coleoptera Curculionidae). *Systematic Entomology* 15:283-296.

Chown, S.L. & Scholtz, C.H. 1989. Biology and ecology of the *Dusmoecetes* Jeannel (Col. Curculionidae) species complex on Marion Island. *Oecologia* 80: 93-99.

Chown S.L. & Smith, V.R. 1993. Climate change and the short-term impact of feral house mice at the sub-Antarctic Prince Edward Islands. *Oecologia* 96: 508-516.

Clement, M., Posada. D. & Crandall, K.A. 2000. TCS: a computer program to estimate gene genealogies. *Molecular Ecology* 9: 1657-1660.

Crandall, K.A. 1996. Multiple Interspecies Transmissions of Humans and Simian T-Cell Leukemia/Lymphoma Virus Type I sequences. *Molecular Biology and Evolution* 13: 115-131.

Crandall, K.A. & Templeton, A.R. 1993. Empirical Tests of Some Predictions From Coalescent Theory With Applications to Intraspecific Phylogeny Reconstruction. *Genetics* 134: 959-969.

Drummond, A.J. & Rambaut, A. 2007. BEAST: Bayesian evolutionary analysis by sampling trees. *BMC Evolutionary Biology* 7: 214.

Excoffier, L. 2004. Patterns of DNA sequence diversity and genetic structure after a range expansion: lessons from the infinite-island model. *Molecular Ecology* 13: 853–864.

Excoffier, L., Smouse, P. & Quattro, J. 1992 Analysis of molecular variance inferred from metric distances among DNA haplotypes: Application to human mitochondrial DNA restriction data. *Genetics* 131:479-491.

Excoffier, L. & Lischer, H.E.L. 2010. Arlequin suite ver 3.5: A new series of programs to perform population genetics analyses under Linux and Windows. *Molecular Ecology Resources* 10: 564-567.

Excoffier, L. & Schneider, S. 1999. Why hunter-gatherer populations do not show signs of Pleistocene demographic expansions. *Proceedings of the National Academy of Sciences of the United States of America* 96: 10597-10602.

Felsenstein, J. 1981. Evolutionary trees from DNA sequences: A maximum likelihood approach. *Journal of Molecular Evolution* 17: 368-376.

Felsenstein, J. 1988. Phylogenies from molecular sequences: Inference and reliability. *Annual Reviews in Genetics* 22: 521-565.

Fu, Y.X. 1997. Statistical tests of neutrality of mutations against population growth, hitchhiking and background selection. *Genetics* 143: 557-570.

Graur, D. & Martin, W. 2004. Reading the entrails of chickens: molecular timescales of evolution and the illusion of precision. *Trends in Genetics* 20: 80-86.

Grobler, G.C., Janse van Rensburg, L., Bastos, A.D.S., Chimimba, C.T. & Chown, S.L. 2006. Molecular and morphometric assessment of the taxonomic status of *Ectemnorhinus* weevil species (Coleoptera: Curculionidae, Entiminae) from the sub-Antarctic Prince Edward Islands. *Journal of Zoological Systematics and Evolutionary Research* 44: 200-211.

Grobler, G.C., Bastos, A.D.S., Treasure, A. & Chown, S.L. 2011. Cryptic species, biogeographic complexity and evolutionary history of the *Ectemnorhinus*-group in the sub-Antarctic, including a description of *Bothrometopus huntleyi*, n. sp. *Antarctic Science* 23: 211-224.

Grobler, G.C., L., Bastos, A.D.S., Chimimba, C.T. & Chown, S.L. 2011. Inter-island dispersal of flightless *Bothrometopus huntleyi* (Coleoptera: Curculionidae) from the sub-Antarctic Prince Edward Island Archipelago. *Antarctic Science* 23: 225-234.

Guindon, S. & Gascuel, O. 2003. A simple, fast and accurate method to estimate large phylogenies by maximum-likelihood. *Systematic Biology* 52: 696-704.

Hall, K.J. 1978. Evidence for Quaternary glaciation of Marion Island (Sub-Antarctic) and some implications. In Van Zinderen Bakker E.M. (ed.) *Antarctic Glacial History and World Palaeo-environments.* A.A. Balkema, Rotterdam, pp. 137-147.

Hall, K. 1980. Late glacial ice cover and palaeotemperatures on sub-Antarctic Marion Island. *Palaeogeography, Palaeoclimatology and Palaeoecology* 29: 243-259.

Hall, K. 1981. Quantitative analysis of till lithology on Marion Island. *South African Journal of Science* 77: 86-90.

Hall, K. 1982. Rapid deglaciation as an initiator of volcanic activity: an hypothesis. *Earth Surface Processes and Landforms* 7: 45-51.

Hall, K. 2004. Quaternary glaciation of the sub-Antarctic Islands. In Ehlers J. & Gibbard P.I. (Eds.). *Quaternary Glaciations - Extent and Chronology, Part III*. Elsevier, Amsterdam, pp. 339-345.

Harley, E.H. 2000. Dapsa 4.9. Department of Chemical Pathology, University of Cape town.

Holsinger, K.E & Weir, B.S. 2009. Genetics in geographically structured populations: defining, estimating and interpreting FST. *Nature Reviews Genetics*, 10: 639-650.

Hudson, R.R., Slatkin, M. & Maddison W.P. 1992. Estimation of levels of gene flow from DNA sequence data. *Genetic*s 132: 583-589.

Huelsenbeck, J.P. & Ronquist, F. 2001. MRBAYES: Bayesian inference of phylogeny. *Bioinformatics*, 17: 754-755.

Jeannel, R. 1940. Coléoptères. Croisière du Bougainville aux îles australes francaises. *Mémoires du Muséum National d'Histoire Naturelle (N.S.)* 14: 63-201.

Jukes, T.H. & Cantor, C.R. 1969. Evolution of protein molecules. In Munro, H.N., editor, *Mammalian Protein Metabolism*, pp. 21-132, Academic Press, New York.

Knowles, L.L. 2008. Why does a method that fails continue to be used? *Evolution* 62: 2713–2717.

Knowles, L.L., & Maddison, W.P. 2002. Statistical phylogeography. *Molecular Ecology* 11: 2623–2635.

Kumar, S. 1996. PHYLTEST: A Program for Testing Phylogenetic Hypothesis, Version 2.0. Institute of Molecular Evolutionary Genetics and Department of Biology. The Pennsylvania State University, University Park, Pennsylvania, USA.

Kuschel, G. & Chown, S.L. 1995. Phylogeny and Systematics of the *Ectemnorhinus*-group of Genera (Insecta: Coleoptera). *Invertebrate Taxonomy* 9: 841-863.

Langenegger, O. & Verwoerd, W.J. 1971. Topographic Survey. Report on the South African biological and geological expedition 1965-1966, In: *Marion and Prince Edward Islands*, van Zinderen Bakker EM, Winterbottom JM, Dryer RA (eds). Cape Town, A. A. Balkema, pp 32-39.

Li, P. & Bousquet, J. 1992. Relative-Rate test for nucleotide substitutions between two lineages. *Molecular Biology and Evolution* 9: 1185-1189.

Librado, P. & Rozas, J. 2009. DnaSP v5: A software for comprehensive analysis of DNA polymorphism data. *Bioinformatics* 25: 1451-1452.

Lynch, M. & Crease T.J. 1990. The analysis of population survey data on DNA sequence variation. *Molecular Biology and Evolution* 7: 377-394.

Mahoney, J., Le Roux, A.P., Peng, Z., Fisher, R.L., & Natland, J.H. 1992. Southwestern limits of Indian Ocean ridge mantle and the origin of low $^{206}Pb/^{204}Pb$ mid-ocean ridge basalt: Isotope systematics of the central Southwest Indian Ridge (17º-50ºE). *Journal of Geophysical Research* 97: 19771-19790.

McCarthy, C. 1996-1997. School of Biomolecular and Biomedical Science, Faculty of Science and Technology, Griffith University, Brisbane, Queensland, Australia.McDougall, I., Verwoerd, W. & Chevallier, L. 2001. K-Ar geochronology of Marion Island, Southern Ocean. *Geological Magazine* 138: 1-17.

McDougall, I., Verwoerd, W. & Chevallier, L. 2001. K-Ar geochronology of Marion Island, Southern Ocean. *Geological Magazine*, 138, 1-17.

Meiklejohn, K.I. & Hedding, D.W. 2005. Marion Island. In: Wunderman, R., Venzke, E. & Mayberry, G. (Eds.). *Bulletin of the Global Volcanism Network*, 30: 16.

Nei, M & Li, W.H. 1979. Mathematical model for studying genetic variation in terms of restriction endonucleases. *Proceedings of the National Academy of Sciences of the United States of America* 76: 5269-5273.

Papadopoulou, A., Anastasiou, I. & Vogler, A.P. 2010. Revisiting the molecular clock: the mid-Aegean trench calibration. *Molecular Biology and Evolution* 27: 1659-1672.

Posada, D. 2008. jModelTest: Phylogenetic Model Averaging. *Molecular Biology and Evolution* 25: 1253-1256.

Posada, D., Crandall, K.A. & Templeton, A.R. 2000. GeoDis: a program for the cladistic nested analysis of the geographical distribution of genetic haplotypes. *Molecular Ecology* 9: 487-488.

Ray, N., Currat, M. & Excoffier, L. Intra-Deme Molecular Diversity in Spatially Expanding Populations. *Molecular Biology and Evolution* 20: 76–86.

Reynolds, J., Weir, B.S. & Cockerham, C.C. 1983. Estimation of the coancestry coefficient: basis for a short-term genetic distance. *Genetics* 105: 767-779.

Rice, W.R. 1984. Disruptive selection on habitat preference and the evolution of reproductive isolation: a simulation study. *Evolution* 38: 1251-1260.

Rogers, R.A. & Harpending, H. 1992. Population Growth Makes Waves in the Distrubution of Pairwise Genetic Differences. *Molecular Biology and Evolution* 9: 552-569.

Rzhetsky, A. & Nei, M. 1992. A simple method for estimating and testing minimum-evolution trees. *Molecular Biology and Evolution* 9: 945-967.

Saitou, N. & Neim M. 1987. The Neighbor-joining Method: A New Method for Reconstructing Phylogenetic Trees. *Molecular Biology and Evolution* 4: 406-425.

Schulze, B.R. 1971. The climate of Marion Island. In: Van Zinderen Bakker, E.M., Winterbottom, J.M. & Dyer, R.A., (eds.) *Marion and Prince Edward Islands: Report on the South African Biological and Geological Expedition 1965-1966.* A.A. Balkeman, Cape Town, pp. 16-31.

Slatkin, M. 1991. Inbreeding coefficients and coalescence times. *Genetic Research, Cambridge* 58: 167-175.

Slatkin, M. 1995. A measure of population subdivision based on microsatellite allele frequencies. *Genetics* 139: 457-462.

Smith, V.R. 2002. Climate change in the sub-Antarctic: An illustration from Marion Island. *Climate Change* 52: 345-357.

Smith, V.R., Avenant, N.L. & Chown, S.L. 2002. The diet and impact of house mice on a sub-Antarctic island. *Polar Biology* 25: 703-715.

Sumner, P.D., Meiklejohn, K.I., Boelhouwers, J.C. & Hedding, D.W. 2004. Climate change melts Marion Island's snow and ice. *South African Journal of Science* 100: 1-4.

Tamura, K. & Nei, M. 1993. Estimation of the number of nucleotide substitutions in the control region of mitochondrial DNA in humans and chimpanzees. *Molecular Biology and Evolution* 10: 512-526.

Tamura, K., Dudley, J., Nei, M. & Kumar, S. 2007. MEGA4: Molecular Evolutionary Genetics Analysis (MEGA) software version 4.0. *Molecular Biology and Evolution* 24: 1596-1599.

Tajima, F. 1983. Evolutionary relationship of DNA sequences in finite populations. *Genetics* 105: 437-460.

Templeton, A.R., 2008. Why does a method that fails continue to be used? The answer. *Evolution* 63: 807–812.

Templeton, A.R., Boerwinkle, E. & Sing, C.F. 1987. A cladistic analyses of phenotypic associations with haplotypes inferred from restriction endonuclease mapping. I. Basic theory and an analysis af alcohol dehydrogenase activity in Droaophila. *Genetics* 117: 343-351.

Templeton, A.R., Crandall, K.A. & Sing, C.F. 1992. A caldistic analysis of phenotypic associations with haplotypes inferred from restriction endonuclease mapping. III. Cladogram estimation. *Genetics* 132: 619-633.

Templeton, A.R., Routman, E. & Phillips, C.A. 1995. Separating population structure from population history: a cladistic analysis of the geographical distribution of mitochondrial DNA haplotypes in the Tiger Salamander, *Ambysoma Tigrinum*. *Genetics*, 134: 659-669.

Templeton, A.R. & Sing, C.F. 1993. A Cladistic Analyses of Phenotypic Associations with Haplotypes Inferred from Restriction Endonuclease Mapping. IV. Nested Analyses with Cladogram Uncertainty and Recombination. *Genetics* 134: 659- 669.

Van Zinderen Bakker, E.M. 1973. The glaciation(s) of Marion Island (sub-Antarctic). In *Palaeoecology of Africa and the Surrounding Islands and Antarctica*, vol. 8, ed. van Zinderen Bakker, E.M., pp. 161-178.

Verwoerd, W.J. 1971. Geology. Report on the South African biological and geological expedition 1965-1966, In: *Marion and Prince Edward Islands*, van Zinderen Bakker, E.M., Winterbottom, J.M. & Dryer, R.A. (eds). Cape Town, A. A. Balkema, pp 40-62.

Verwoerd, W.J., Russell, S., & Berruti, A. 1981. 1980 Volcanic eruption reported on Marion Island. *Earth and Planetary Science Letters* 54: 153-156.

Waterhouse, G.R. 1853. Descriptions of new genera and species of Culculionides. *Transactions of the Entomological Society of London* 2: 172-207.

Waterhouse, C.O. 1885. Description of two new Curculionidae (*Ectemnorhinus*) from Marion Islands. *Annals and Magazine of Natural History, London* 16: 121-123.

Wright, S. 1951. The genetical structure of populations. *Annals of Eugenics* 15: 323-354.

Appendix 1: Map showing sample sites on Marion Island, in green, and on Prince Edward Island, in red.

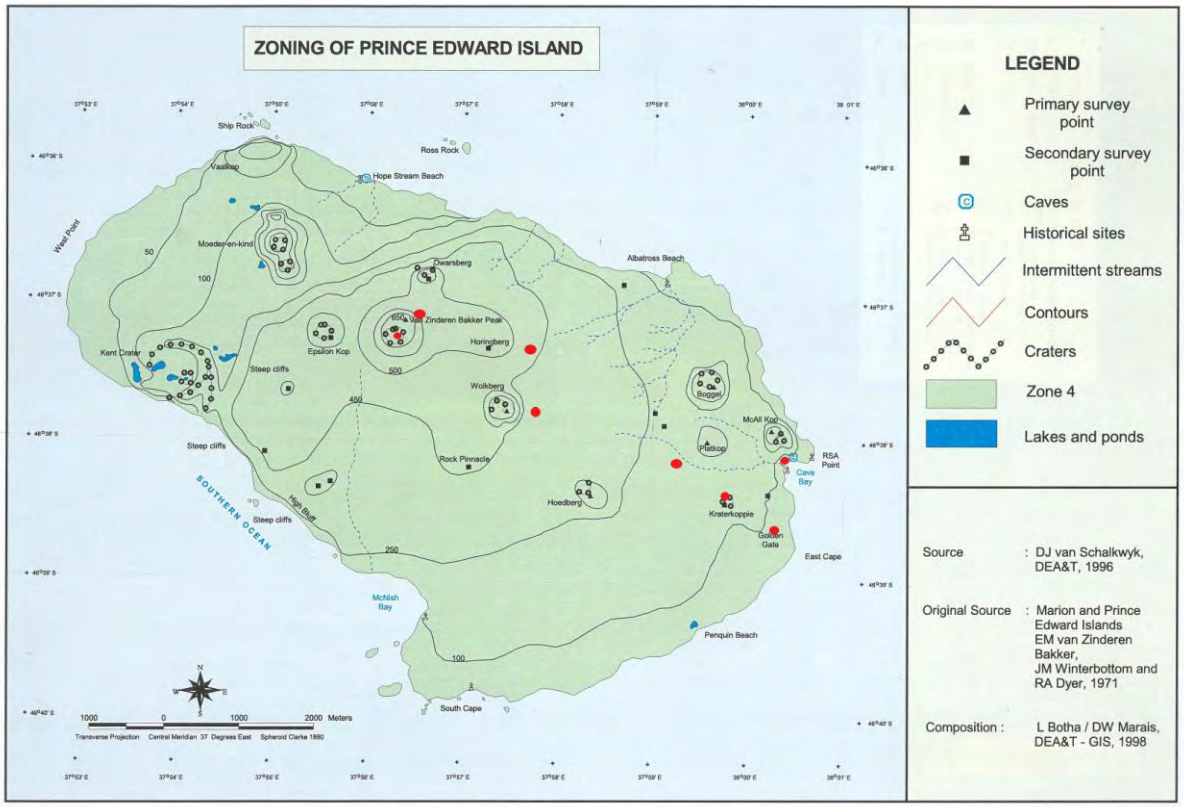

Appendix II: Summary of the sampling localities on Marion (MI) and Prince Edward Islands (PEI) from which the genetically characterised specimens included in this study were collected.

Island	Sampling Locality (a.s.l)	Geographic coordinates	Voucher	Species	GenBank
MI	Halfway Kop (600 m)	S 46º54'06'' E 37º47'83''	125-4	*E. similis*	JF327538
MI	Halfway Kop (600 m)	S 46º54'06'' E 37º47'83''	126-1	*E. similis*	JF327559
MI	Halfway Kop (600 m)	S 46º54'06'' E 37º47'83''	126-52	*E. similis*	JF327560
MI	Halfway Kop (600 m)	S 46º54'06'' E 37º47'83''	125-51	*E. similis*	JF327566
MI	Halfway Kop (600 m)	S 46º54'06'' E 37º47'83''	126-6	*E. similis*	JF327561
MI	Halfway Kop (600 m)	S 46º54'06'' E 37º47'83''	125-42	*E. similis*	JF327562
MI	Halfway Kop (600 m)	S 46º54'06'' E 37º47'83''	125-43	*E. similis*	JF327539
MI	Halfway Kop (600 m)	S 46º54'06'' E 37º47'83''	125-53	*E. similis*	JF327630
MI	Albatros Lakes (50 m)	S 46º53'49.2'' E 37º51'55''	110-27	*E. similis*	AY762288
MI	Albatros Lakes (50 m)	S 46º53'49.2'' E 37º51'55''	110-3	*E. similis*	AY762287
MI	Albatros Lakes (50 m)	S 46º53'49.2'' E 37º51'55''	110-18	*E. similis*	AY762294
MI	Albatros Lakes (50 m)	S 46º53'49.2'' E 37º51'55''	84-2	*E. similis*	JF327626
MI	Albatros Lakes (50 m)	S 46º53'49.2'' E 37º51'55''	110-29	*E. similis*	JF327563
MI	Albatros Lakes (50 m)	S 46º53'49.2'' E 37º51'55''	110-36	*E. similis*	AY762289
MI	Albatros Lakes (50 m)	S 46º53'49.2'' E 37º51'55''	84-1	*E. similis*	JF327616
MI	Albatros Lakes (50 m)	S 46º53'49.2'' E 37º51'55''	84-14	*E. similis*	JF327609
MI	Skua Ridge (100 m)	S 46º51'50'' E 37º51'486''	70-4	*E. similis*	JF327624
MI	Skua Ridge (100 m)	S 46º51'50'' E 37º51'486''	65-3	*E. similis*	JF327627
MI	Skua Ridge (100 m)	S 46º51'50'' E 37º51'486''	68-38	*E. similis*	JF327625
MI	Skua Ridge (100 m)	S 46º51'50'' E 37º51'486''	68-32	*E. similis*	JF327607
MI	Long Ridge South (450 m)	S 46°52'45'' E 37°47'00''	353-7	*E. similis*	JF327592
MI	Long Ridge South (450 m)	S 46°52'45'' E 37°47'00''	353-2	*E. similis*	JF327591
MI	Long Ridge South (450 m)	S 46°52'45'' E 37°47'00''	354-14	*E. similis*	JF327593
MI	Tate's Hill (400m)	S 46º54'36'' E 37º50'28.68''	120-20	*E. similis*	AY762293
MI	Tate's Hill (400m)	S 46º54'36'' E 37º50'28.68''	121-7	*E. similis*	JF327526
MI	Tate's Hill (400m)	S 46º54'36'' E 37º50'28.68''	121-1	*E. similis*	JF327525
MI	Tate's Hill (400m)	S 46º54'36'' E 37º50'28.68''	120-2	*E. similis*	AY762290
MI	Tate's Hill (400m)	S 46º54'36'' E 37º50'28.68''	120-10	*E. similis*	AY762267
MI	Tate's Hill (400m)	S 46º54'36'' E 37º50'28.68''	120-16	*E. similis*	JF327508
MI	Tate's Hill (400m)	S 46º54'36'' E 37º50'28.68''	120-18	*E. similis*	AY762291
MI	Tate's Hill (400m)	S 46º54'36'' E 37º50'28.68''	121-16	*E. similis*	JF327523
MI	Tate's Hill (400m)	S 46º54'36'' E 37º50'28.68''	122-16	*E. similis*	JF327522
MI	Tate's Hill (400m)	S 46º54'36'' E 37º50'28.68''	122-19	*E. similis*	JF327521
MI	Tate's Hill (400m)	S 46º54'36'' E 37º50'28.68''	120-7	*E. similis*	JF327564
MI	Tate's Hill (400m)	S 46º54'36'' E 37º50'28.68''	121-3	*E. similis*	JF327524
MI	Tafelberg (250 m)	S 46°53'03.5'' E 37°48'20.1''	24-3	*E. similis*	JF327623
MI	Tafelberg (250 m)	S 46°53'03.5'' E 37°48'20.1''	24-4	*E. similis*	JF327621
MI	Tafelberg (250 m)	S 46°53'03.5'' E 37°48'20.1''	35-9	*E. similis*	JF327610
MI	Tafelberg (250 m)	S 46°53'03.5'' E 37°48'20.1''	37-4	*E. similis*	JF327605
MI	Tafelberg (250 m)	S 46°53'03.5'' E 37°48'20.1''	23-4	*E. similis*	JF327613
MI	Tafelberg (250 m)	S 46°53'03.5'' E 37°48'20.1''	37-6	*E. similis*	JF327612
MI	Katedraal Krans (800 m)	S 46°53'89.6'' E 37°46'48.2''	163-17	*E. similis*	AY762269
MI	Katedraal Krans (800 m)	S 46°53'89.6'' E 37°46'48.2''	167-22	*E. similis*	AY762272
MI	Katedraal Krans (800 m)	S 46°53'89.6'' E 37°46'48.2''	164-10	*E. similis*	JF327629
MI	Katedraal Krans (800 m)	S 46°53'89.6'' E 37°46'48.2''	164-9	*E. similis*	AY762268

Island	Sampling Locality (a.s.l)	Geographic coordinates	Voucher	Species	GenBank
MI	Katedraal Krans (800 m)	S 46°53’89.6’’ E 37°46’48.2’’	163-32	*E. similis*	JF327541
MI	Katedraal Krans (800 m)	S 46°53’89.6’’ E 37°46’48.2’’	163-31	*E. similis*	AY762292
MI	Katedraal Krans (800 m)	S 46°53’89.6’’ E 37°46’48.2’’	163-2	*E. similis*	AY762270
MI	Junior's Kop (200 m)	S 46°52’79.4’’ E 37°50’08.3’’	150-1	*E. similis*	AY762285
MI	Junior's Kop (200 m)	S 46°52’79.4’’ E 37°50’08.3’’	150-10	*E. similis*	JF327546
MI	Junior's Kop (200 m)	S 46°52’79.4’’ E 37°50’08.3’’	150-4	*E. similis*	AY762284
MI	Junior's Kop (200 m)	S 46°52’79.4’’ E 37°50’08.3’’	149-26	*E. similis*	JF327545
MI	Junior's Kop (200 m)	S 46°52’79.4’’ E 37°50’08.3’’	149-38	*E. similis*	AY762286
MI	Junior's Kop (200 m)	S 46°52’79.4’’ E 37°50’08.3’’	149-32	*E. similis*	AY762283
MI	First Red Hill (400 m)	S 46°53’41.2’’ E 37°48’21’’	173-1	*E. similis*	AY762281
MI	First Red Hill (400 m)	S 46°53’41.2’’ E 37°48’21’’	173-2	*E. similis*	AY762280
MI	First Red Hill (400 m)	S 46°53’41.2’’ E 37°48’21’’	172-18	*E. similis*	JF327544
MI	First Red Hill (400 m)	S 46°53’41.2’’ E 37°48’21’’	172-73	*E. similis*	AY762279
MI	First Red Hill (400 m)	S 46°53’41.2’’ E 37°48’21’’	172-16	*E. similis*	AY762282
MI	First Red Hill (600 m)	S 46º53’39.82’’ E 37º47’12.48’’	168-4	*E. similis*	AY762274
MI	First Red Hill (600 m)	S 46º53’39.82’’ E 37º47’12.48’’	168-5	*E. similis*	AY762273
MI	First Red Hill (600 m)	S 46º53’39.82’’ E 37º47’12.48’’	167-15	*E. similis*	JF327542
MI	First Red Hill (600 m)	S 46º53’39.82’’ E 37º47’12.48’’	167-7	*E. similis*	AY762271
MI	Repetto’s Hill (300 m)	S 46º50’35.7’’ E 37º44’21.8’’	140-32	*E. similis*	JF327550
MI	Repetto’s Hill (300 m)	S 46º50’35.7’’ E 37º44’21.8’’	140-33	*E. similis*	JF327536
MI	Repetto’s Hill (300 m)	S 46º50’35.7’’ E 37º44’21.8’’	140-24	*E. similis*	JF327557
MI	Repetto’s Hill (300 m)	S 46º50’35.7’’ E 37º44’21.8’’	140-3	*E. similis*	JF327537
MI	Repetto’s Hill (300 m)	S 46º50’35.7’’ E 37º44’21.8’’	139-4	*E. similis*	JF327558
MI	Repetto’s Hill (300 m)	S 46º50’35.7’’ E 37º44’21.8’’	140-6	*E. similis*	JF327535
MI	Stony Ridge (150 m)	S 46°54’88.1’’ E 37°51’48.4’’	118-14	*E. similis*	JF327540
MI	Stony Ridge (150 m)	S 46°54’88.1’’ E 37°51’48.4’’	119-17	*E. similis*	JF327517
MI	Stony Ridge (150 m)	S 46°54’88.1’’ E 37°51’48.4’’	118-9	*E. similis*	JF327519
MI	Stony Ridge (150 m)	S 46°54’88.1’’ E 37°51’48.4’’	118-3	*E. similis*	JF327551
MI	Stony Ridge (150 m)	S 46°54’88.1’’ E 37°51’48.4’’	118-10	*E. similis*	JF327506
MI	Stony Ridge (150 m)	S 46°54’88.1’’ E 37°51’48.4’’	44-12	*E. similis*	JF327617
MI	Stony Ridge (150 m)	S 46°54’88.1’’ E 37°51’48.4’’	119-29	*E. similis*	JF327518
MI	Stony Ridge (150 m)	S 46°54’88.1’’ E 37°51’48.4’’	46-9	*E. similis*	JF327619
MI	Stony Ridge (150 m)	S 46°54’88.1’’ E 37°51’48.4’’	119-7	*E. similis*	JF327520
MI	Stony Ridge (150 m)	S 46°54’88.1’’ E 37°51’48.4’’	44-15	*E. similis*	JF327614
MI	Van Den Boogaard (150 m)	S 46º52’46.3’’ E 37º49’58.1’’	75-16	*E. similis*	JF327628
MI	Van Den Boogaard (150 m)	S 46º52’46.3’’ E 37º49’58.1’’	75-2	*E. similis*	JF327622
MI	Lou-se-kop (150 m)	S 46º49’49.44’’ E 37º42’47.52’’	136-11	*E. similis*	JF327565
MI	Lou-se-kop (150 m)	S 46º49’49.44’’ E 37º42’47.52’’	136-39	*E. similis*	JF327554
MI	Lou-se-kop (150 m)	S 46º49’49.44’’ E 37º42’47.52’’	137-3	*E. similis*	JF327510
MI	Lou-se-kop (150 m)	S 46º49’49.44’’ E 37º42’47.52’’	137-2	*E. similis*	JF327511
MI	Lou-se-kop (150 m)	S 46º49’49.44’’ E 37º42’47.52’’	136-61	*E. similis*	JF327509
MI	Johnny’s Hill (300 m)	S 46º57’50’’ E 37º49’30’’	335-2	*E. similis*	JF327568
MI	Johnny’s Hill (300 m)	S 46º57’50’’ E 37º49’30’’	336-26	*E. similis*	JF327571
MI	Johnny’s Hill (300 m)	S 46º57’50’’ E 37º49’30’’	336-18	*E. similis*	JF327570
MI	Johnny’s Hill (300 m)	S 46º57’50’’ E 37º49’30’’	335-3	*E. similis*	JF327569
MI	Cape Davis (0 m)	S 46°49’41.2’’ E 37°41’83.3’’	138-8	*E. similis*	JF327513
MI	Cape Davis (0 m)	S 46°49’41.2’’ E 37°41’83.3’’	138-7	*E. similis*	JF327527

Island	Sampling Locality (a.s.l)	Geographic coordinates	Voucher	Species	GenBank
MI	Cape Davis (0 m)	S 46°49'41.2'' E 37°41'83.3''	134-3	*E. similis*	JF327514
MI	Cape Davis (0 m)	S 46°49'41.2'' E 37°41'83.3''	134-2	*E. similis*	JF327553
MI	Cape Davis (0 m)	S 46°49'41.2'' E 37°41'83.3''	138-5	*E. similis*	JF327552
MI	Cape Davis (0 m)	S 46°49'41.2'' E 37°41'83.3''	134-4	*E. similis*	JF327515
MI	Cape Davis (0 m)	S 46°49'41.2'' E 37°41'83.3''	134-5	*E. similis*	JF327516
MI	Cape Davis (0 m)	S 46°49'41.2'' E 37°41'83.3''	138-6	*E. similis*	JF327512
MI	Azorellakop (450 m)	S 46º52'2.1'' E 37º39'57.3''	142-7	*E. similis*	JF327530
MI	Azorellakop (450 m)	S 46º52'2.1'' E 37º39'57.3''	142-9	*E. similis*	JF327556
MI	Azorellakop (450 m)	S 46º52'2.1'' E 37º39'57.3''	143-7	*E. similis*	JF327534
MI	Azorellakop (450 m)	S 46º52'2.1'' E 37º39'57.3''	143-14	*E. similis*	JF327533
MI	Azorellakop (450 m)	S 46º52'2.1'' E 37º39'57.3''	143-15	*E. similis*	JF327532
MI	Azorellakop (450 m)	S 46º52'2.1'' E 37º39'57.3''	143-9	*E. similis*	JF327531
MI	Azorellakop (450 m)	S 46º52'2.1'' E 37º39'57.3''	142-1	*E. similis*	JF327529
MI	Ice Plateau (1000 m)	S 46º54'17.4'' E 37º45'22.5''	157-8	*E. similis*	AY762276
MI	Ice Plateau (1000 m)	S 46º54'17.4'' E 37º45'22.5''	157-5	*E. similis*	JF327567
MI	Ice Plateau (1000 m)	S 46º54'17.4'' E 37º45'22.5''	157-4	*E. similis*	JF327543
MI	Ice Plateau (1000 m)	S 46º54'17.4'' E 37º45'22.5''	157-3	*E. similis*	AY762278
MI	Ice Plateau (1000 m)	S 46º54'17.4'' E 37º45'22.5''	157-12	*E. similis*	AY762277
MI	Ice Plateau (1000 m)	S 46º54'17.4'' E 37º45'22.5''	157-2	*E. similis*	AY762275
MI	Kildalkey Bay (0 m)	S 46°57'38.3'' E 37°51'22.2''	332-9	*E. similis*	JF327585
MI	Kildalkey Bay (0 m)	S 46°57'38.3'' E 37°51'22.2''	332-14	*E. similis*	JF327586
MI	Kildalkey Bay (0 m)	S 46°57'38.3'' E 37°51'22.2''	332-7	*E. similis*	JF327583
MI	Kildalkey Bay (0 m)	S 46°57'38.3'' E 37°51'22.2''	332-1	*E. similis*	JF327584
MI	Water Tunnel (0 m)	S 46°57'49.2'' E 37°44'50.44''	343-13	*E. similis*	JF327602
MI	Water Tunnel (0 m)	S 46°57'49.2'' E 37°44'50.44''	343-25	*E. similis*	JF327573
MI	Water Tunnel (0 m)	S 46°57'49.2'' E 37°44'50.44''	343-17	*E. similis*	JF327572
MI	Transvaal Cove Base (0 m)	S 46º52'36.6'' E 37º51'35.94''	55-26	*E. similis*	JF327620
MI	Transvaal Cove Base (0 m)	S 46º52'36.6'' E 37º51'35.94''	55-34	*E. similis*	JF327618
MI	Sidney Hill (300 m)	S 46º57'34.7'' E 37º39'53.2''	359-3	*E. similis*	JF327579
MI	Sidney Hill (300 m)	S 46º57'34.7'' E 37º39'53.2''	360-17	*E. similis*	JF327581
MI	Sidney Hill (300 m)	S 46º57'34.7'' E 37º39'53.2''	359-5	*E. similis*	JF327580
MI	Sidney Hill (300 m)	S 46º57'34.7'' E 37º39'53.2''	360-14	*E. similis*	JF327582
MI	Swartkop (50 m)	S 46º55'26.94'' E 37º35'43.86''	145-24	*E. similis*	JF327555
MI	Swartkop (50 m)	S 46º55'26.94'' E 37º35'43.86''	145-34	*E. similis*	JF327507
MI	Swartkop (50 m)	S 46º55'26.94'' E 37º35'43.86''	146-12	*E. similis*	JF327549
MI	Swartkop (50 m)	S 46º55'26.94'' E 37º35'43.86''	145-19	*E. similis*	JF327528
MI	Swartkop (50 m)	S 46º55'26.94'' E 37º35'43.86''	146-13	*E. similis*	JF327548
MI	Swartkop (50 m)	S 46º55'26.94'' E 37º35'43.86''	146-8	*E. similis*	JF327547
MI	Feldmark Plateau (600 m)	S 46°56'35'' E 37°46'10''	337-23	*E. similis*	JF327587
MI	Feldmark Plateau (600 m)	S 46°56'35'' E 37°46'10''	337-26	*E. similis*	JF327588
MI	Feldmark Plateau (600 m)	S 46°56'35'' E 37°46'10''	338-2	*E. similis*	JF327589
MI	Feldmark Plateau (600 m)	S 46°56'35'' E 37°46'10''	338-4	*E. similis*	JF327590
MI	Pyroxene Kop (600 m)	S 46°56'43.4'' E 37°41'40.5''	346-27	*E. similis*	JF327600
MI	Pyroxene Kop (600 m)	S 46°56'43.4'' E 37°41'40.5''	346-17	*E. similis*	JF327574
MI	Pyroxene Kop (600 m)	S 46°56'43.4'' E 37°41'40.5''	348-2	*E. similis*	JF327575
MI	Pyroxene Kop (600 m)	S 46°56'43.4'' E 37°41'40.5''	348-3	*E. similis*	JF327594
MI	Goodhope Bay (0 m)	S 46°57'55.9'' E 37°42'04.4''	353A-3	*E. similis*	JF327577

Island	Sampling Locality (a.s.l)	Geographic coordinates	Voucher	Species	GenBank
MI	Goodhope Bay (0 m)	S 46°57'55.9'' E 37°42'04.4''	352-6	*E. similis*	JF327576
MI	Goodhope Bay (0 m)	S 46°57'55.9'' E 37°42'04.4''	353A-5	*E. similis*	JF327578
MI	Goodhope Bay (0 m)	S 46°57'55.9'' E 37°42'04.4''	352-24	*E. similis*	JF327601
MI	Ship's Cove (0 m)	S 46°51'41'' E 37°50'66''	21-2	*E. similis*	JF327611
MI	Trypot Beach (0 m)	S 46°53'05.2'' E 37°52'06''	14-2	*E. similis*	JF327615
MI	Archway Bay (0 m)	S 46º53'56.9'' E 37º53'45''	78-5	*E. similis*	JF327608
MI	Archway Bay (0 m)	S 46º53'56.9'' E 37º53'45''	78-1	*E. similis*	JF327606
PEI	Cave Bay (0 m)	S 46º38'45.12'' E 37º59'46.8''	304-14	*E. similis*	AY762298
PEI	Cave Bay (0 m)	S 46º38'45.12'' E 37º59'46.8''	304-24	*E. similis*	JF327595
PEI	Cave Bay (0 m)	S 46º38'45.12'' E 37º59'46.8''	304-28	*E. similis*	AY762299
PEI	Cave Bay (0 m)	S 46º38'45.12'' E 37º59'46.8''	304-4	*E. similis*	AY762301
PEI	Cave Bay (0 m)	S 46º38'45.12'' E 37º59'46.8''	304-6	*E. similis*	JF327596
PEI	Cave Bay (0 m)	S 46º38'45.12'' E 37º59'46.8''	304-13	*E. kucheli*	AY762312
PEI	(200 m)	S 46º38'27.42'' E 37º58'23.76''	315-7	*E. similis*	AY762295
PEI	(200 m)	S 46º38'27.42'' E 37º58'23.76''	315-22	*E. similis*	AY762297
PEI	(200 m)	S 46º38'27.42'' E 37º58'23.76''	316-29	*E. similis*	JF327598
PEI	(200 m)	S 46º38'27.42'' E 37º58'23.76''	316-30	*E. kucheli*	JF327637
PEI	(200 m)	S 46º38'27.42'' E 37º58'23.76''	316-6	*E. kucheli*	AY762311
PEI	(200 m)	S 46º38'27.42'' E 37º58'23.76''	316-15	*E. kucheli*	AY762314
PEI	(400 m)	S 46º38'12.66'' E 37º57'28.92''	309-16	*E. similis*	AY762296
PEI	(400 m)	S 46º38'12.66'' E 37º57'28.92''	309-7	*E. kucheli*	AY762316
PEI	(400 m)	S 46º38'12.66'' E 37º57'28.92''	310-4	*E. kucheli*	AY762317
PEI	(400 m)	S 46º38'12.66'' E 37º57'28.92''	310-15	*E. kucheli*	JF327640
PEI	(400 m)	S 46º38'12.66'' E 37º57'28.92''	310-3	*E. kucheli*	AY762318
PEI	(600 m)	S 46º37'31.98'' E 37º55'59.1''	312-10	*E. similis*	AY762302
PEI	(600 m)	S 46º37'31.98'' E 37º55'59.1''	312-16	*E. similis*	JF327597
PEI	(600 m)	S 46º37'31.98'' E 37º55'59.1''	312-5	*E. similis*	AY762305
PEI	(600 m)	S 46º37'31.98'' E 37º55'59.1''	312-6	*E. kucheli*	JF327636
PEI	(600 m)	S 46º37'31.98'' E 37º55'59.1''	311-10	*E. kucheli*	AY762309
PEI	(600 m)	S 46º37'31.98'' E 37º55'59.1''	311-7	*E. kucheli*	AY762310
PEI	TvZB (672 m)	S 46º37'35.4'' E 37º55'53.46''	320-1	*E. similis*	AY762307
PEI	TvZB (672 m)	S 46º37'35.4'' E 37º55'53.46''	321-11	*E. similis*	AY762308
PEI	TvZB (672 m)	S 46º37'35.4'' E 37º55'53.46''	320-3	*E. similis*	AY762306
PEI	TvZB (672 m)	S 46º37'35.4'' E 37º55'53.46''	321-2	*E. kucheli*	AY762315
PEI	TvZB (672 m)	S 46º37'35.4'' E 37º55'53.46''	320-4	*E. kucheli*	JF327638
PEI	Ditrichum (450 m)	S 46º38'3.42'' E 37º56'46.26''	306-1	*E. similis*	AY762300
PEI	Ditrichum (450 m)	S 46º38'3.42'' E 37º56'46.26''	306-7	*E. similis*	JF327599
PEI	Ditrichum (450 m)	S 46º38'3.42'' E 37º56'46.26''	305-3	*E. similis*	AY762303
PEI	Ditrichum (450 m)	S 46º38'3.42'' E 37º56'46.26''	306-4	*E. similis*	AY762304
PEI	Ditrichum (450 m)	S 46º38'3.42'' E 37º56'46.26''	305-2	*E. kucheli*	JF327639
PEI	Ditrichum (450 m)	S 46º38'3.42'' E 37º56'46.26''	305-1	*E. kucheli*	AY762313
PEI	Krater Koppie (150 m)	S 46º38'24.36'' E 37º59'46.92''	18-8	*E. similis*	JF327604
PEI	Krater Koppie (150 m)	S 46º38'24.36'' E 37º59'46.92''	18-7	*E. similis*	JF327603
PEI	Krater Koppie (150 m)	S 46º38'24.36'' E 37º59'46.92''	18-15	*E. kucheli*	JF327631
PEI	Krater Koppie (150 m)	S 46º38'24.36'' E 37º59'46.92''	18-5	*E. kucheli*	JF327635
PEI	Golden Gate (50 m)	S 46º38'35.7'' E 38º00'16.38''	17-14	*E. kucheli*	JF327634
PEI	Golden Gate (50 m)	S 46º38'35.7'' E 38º00'16.38''	14-6	*E. kucheli*	JF327632

Island	Sampling Locality (a.s.l)	Geographic coordinates	Voucher	Species	GenBank
PEI	Golden Gate (50 m)	S 46º38'35.7'' E 38º00'16.38''	17-3	*E. kucheli*	JF327633